SUPPLEMENTARY INFORMATION

Rational Donor Placement into a Native Exciton Manifold: Cavity-Anchored Dyes Drive Sub-Picosecond Energy Transfer in Light-Harvesting Complex 2

Ryoga Morishita,[1] *Rio Tsuji,*[2] *Seiya Takamori,*[1] *Tetsuya Yamamoto,*[3] *Sora Ishikawa,*[3] *Risa Kojima,*[3] *Masaharu Kondo,*[1] *Takeshi Yanai,*[2,4] *Kazuhiro J. Fujimoto,*[*, 2,4] *Yutaka Nagasawa,*[*, 3] *Takehisa Dewa*[*, 1]

[1]Department of Life Science and Applied Chemistry, Graduate School of Engineering, Nagoya Institute of Technology, Gokiso-cho, Showa-ku, Nagoya, Aichi 466-8555, Japan

[2]Department of Chemistry, Graduate School of Science, Nagoya University, Furo-cho, Chikusa-ku, Nagoya, Aichi 464-8601, Japan

[3]College of Life Sciences, Ritsumeikan University, Kusatsu, Shiga 525-8557, Japan

[4]Institute of Transformative Bio-Molecules (WPI-ITbM), Nagoya University, Furo-cho, Chikusa-ku, Nagoya, Aichi 464-8601, Japan

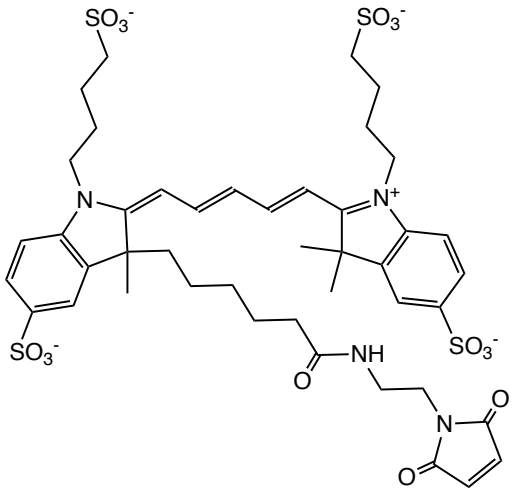

Figure S1. Chemical structure of Alexa647 bearing a thiol-reactive maleimide group.

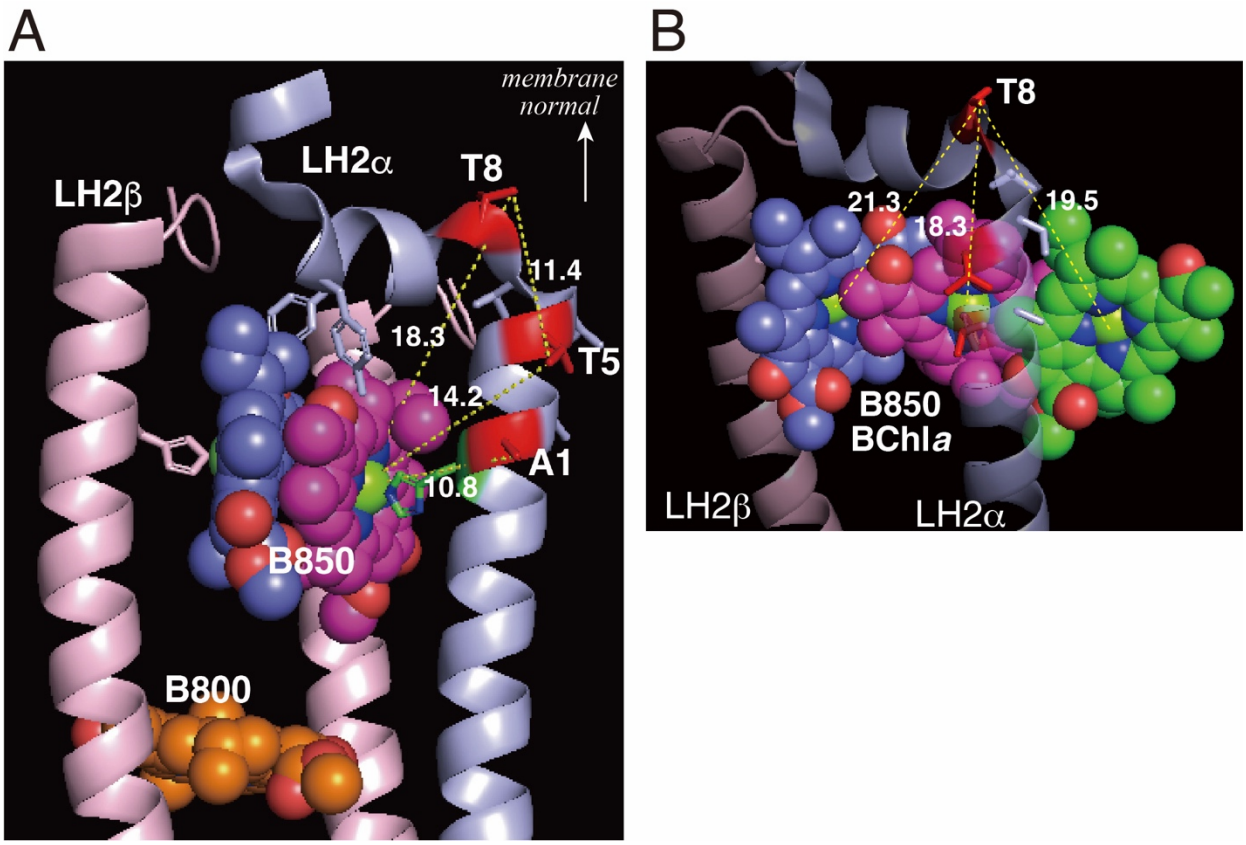

Figure S2. Locations of the mutation sites introduced into the LH2α-polypeptide and their spatial relationships to the B850-BChl*a* pigments. The structural model is based on the wild-type LH2 complex from *Rba. sphaeroides* 2.4.1 (PDB ID: 7PBW). The distances (Å) between the Cβ atom of A1 or Cγ atoms of T5 and T8 and the central Mg atom of the nearest B850-BChl*a* (A), and between the Cγ atom of T8 and Mg atoms of three proximal B850-BChl*a*s (B) are shown. All distances were measured using PyMOL.

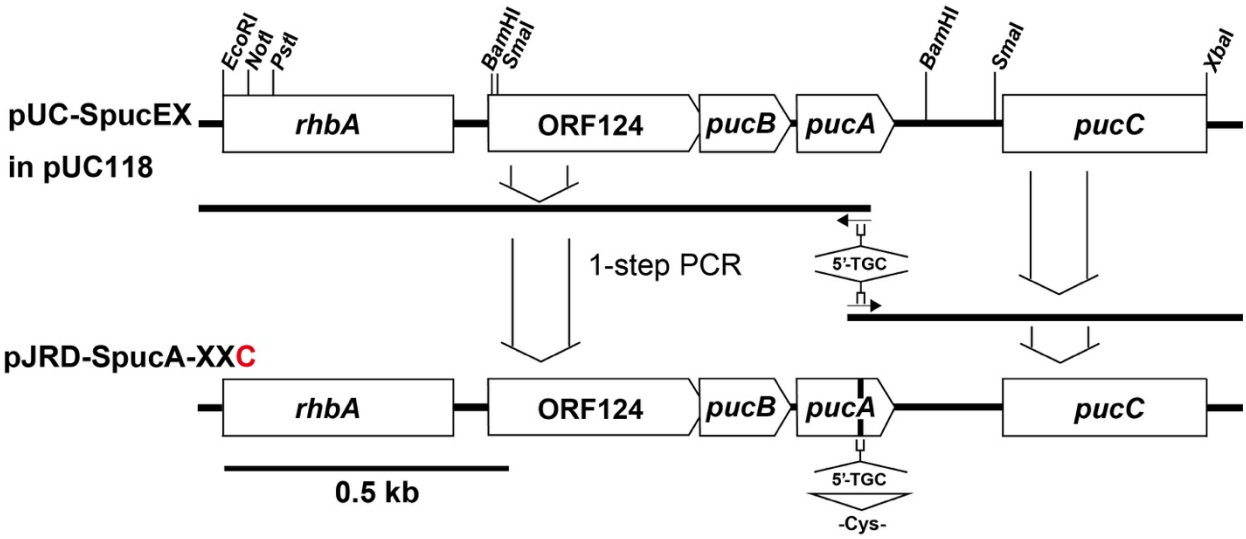

Scheme S1. Schematic overview of the gene manipulations performed in this study.

Table S1. Primers used for the site-directed mutagenesis of the *pucA* gene and for sequencing of *pucBA*

DNA primer	Sequence[a)]
pucA_A1C_F	5'-GTTCACTGCGCTGTGCTGACCACCACC-3'
pucA_A1C_R	5'-CACAGCGCAGTGAACCACAACCGAAGC-3'
pucA_T5C_F	5'-GTGCTGTGCACCACCACCTGGCTGCCC-3'
pucA_T5C_R	5'-GGTGGTGCACAGCACAGCAGCGTGAAC-3'
pucA_T8C_F	5'-ACCACCTGCTGGCTGCCCGACTACTAC-3'
pucA_T8C_R	5'-CAGCCAGCAGGTGGTGGTCAGCACAGC-3'
Seq_pucBA_F	5'-GTCTCGTCGAAGCCCGCGTG-3'
Seq_pucBA_R	5'-CAAGGATCCCGGCCTGCTCGG-3'

[a)] Underlined nucleotides introduce the Cys substitution.

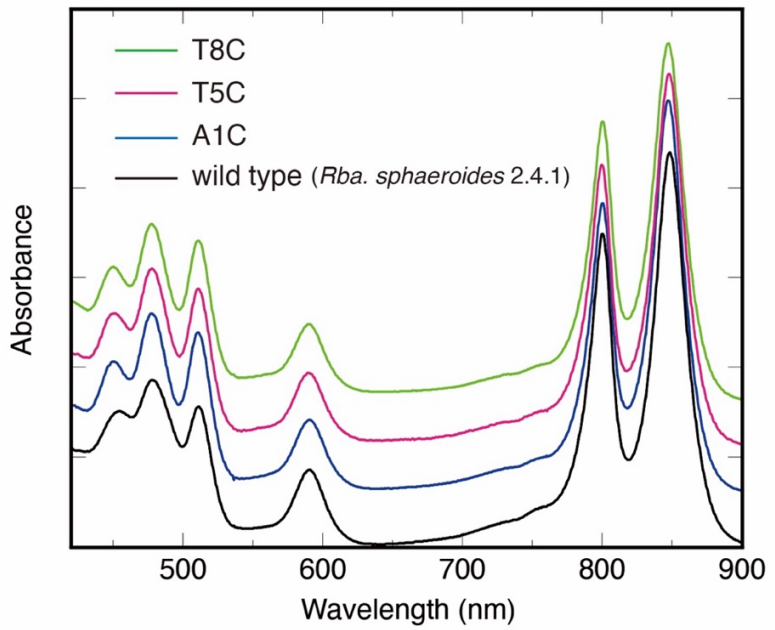

Figure S3. Absorption spectra of wild-type LH2 (*Rba. sphaeroides* 2.4.1; black) and LH2 mutants A1C (blue), T5C (red), and T8C (green). Samples were dissolved in Tris-HCl buffer (20 mM, pH 8.0) containing 0.02 wt % β-DDM.

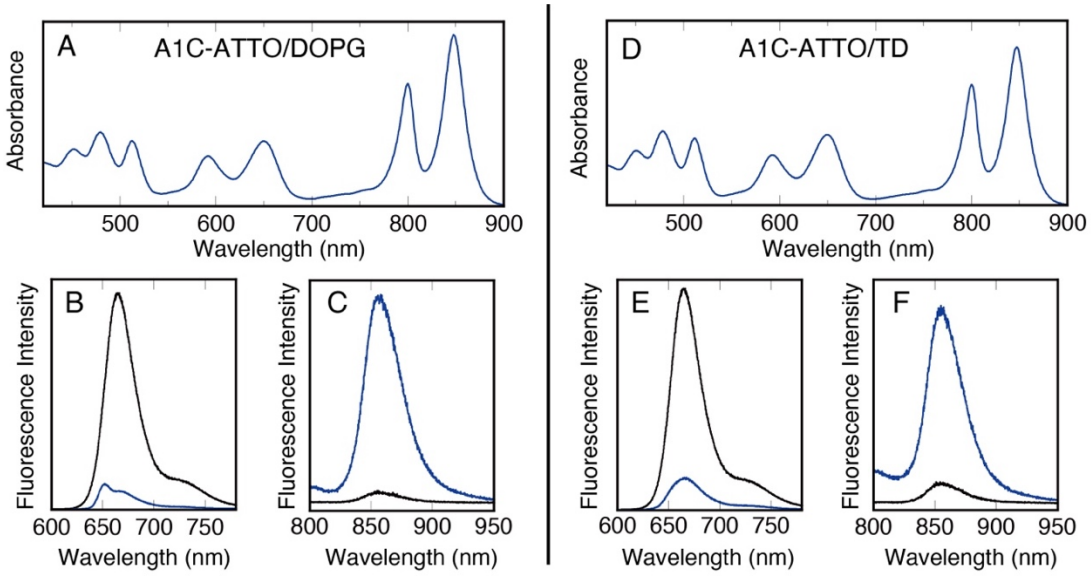

Figure S4. Static absorption and fluorescence spectra of A1C-ATTO in DOPG-reconstituted lipid bilayers (A–C) and in TD buffer (20 mM Tris-HCl, pH 8.0, containing 0.02 wt % β-DDM) (D–F). Fluorescence spectra upon excitation at 650 nm (B, C, E, and F) indicate quenching of ATTO fluorescence (B and E; blue and black traces correspond to A1C-ATTO and free ATTO at the same ATTO concentration as in A1C-ATTO, respectively) and concomitant enhancement of B850 fluorescence (C and F; blue and black traces correspond to A1C-ATTO and A1C at the same LH2 concentration as in A1C-ATTO, respectively).

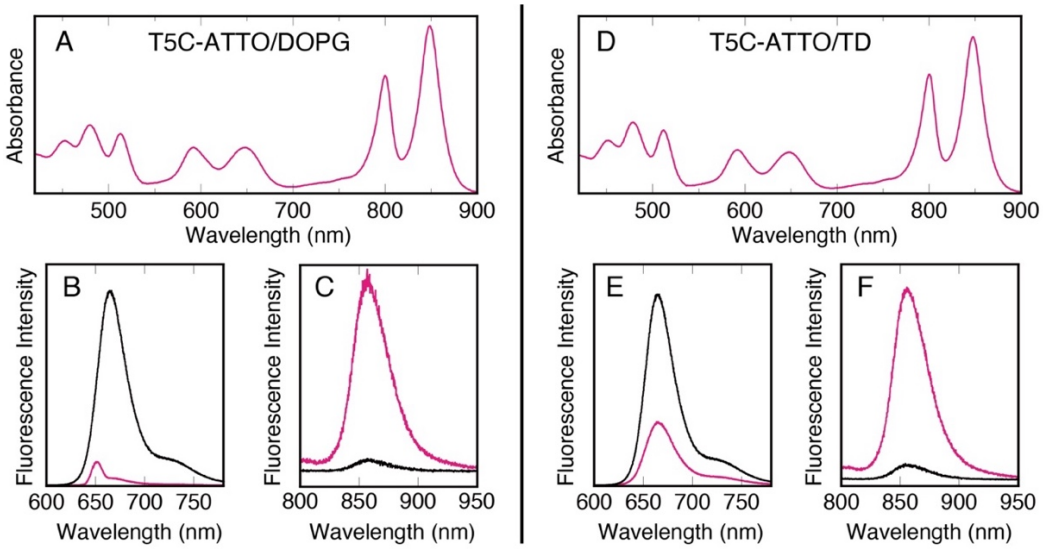

Figure S5. Static absorption and fluorescence spectra of T5C-ATTO in DOPG-reconstituted lipid bilayers (A–C) and in TD buffer (20 mM Tris-HCl, pH 8.0, containing 0.02 wt % β-DDM) (D–F). Fluorescence spectra upon excitation at 650 nm (B, C, E, and F) indicate quenching of ATTO fluorescence (B and E; blue and black traces correspond to T5C-ATTO and free ATTO at the same ATTO concentration as in T5C-ATTO, respectively) and concomitant enhancement of B850 fluorescence (C and F; blue and black traces correspond to T5C-ATTO and T5C at the same LH2 concentration as in T5C-ATTO, respectively).

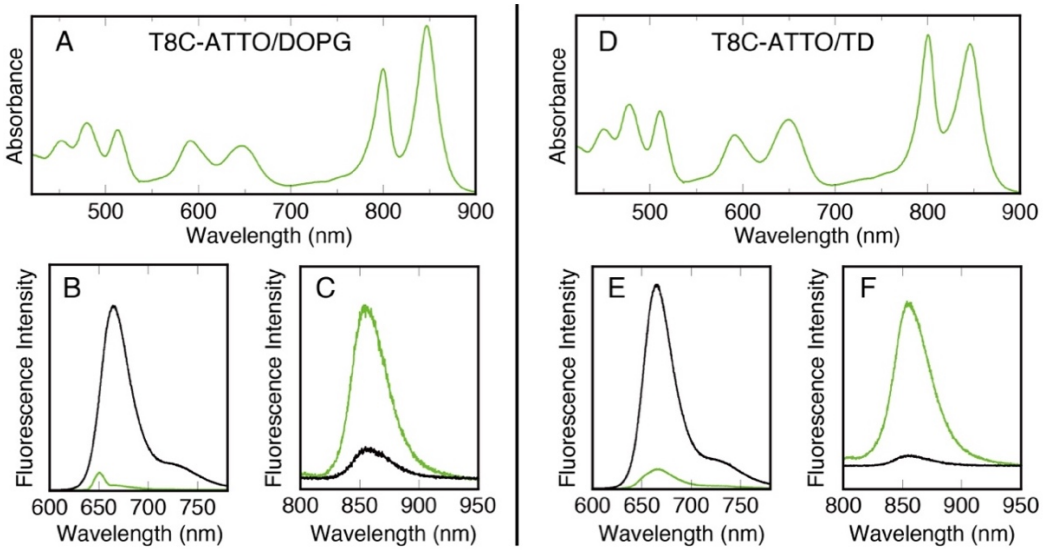

Figure S6. Static absorption and fluorescence spectra of T8C-ATTO in DOPG-reconstituted lipid bilayers (A–C) and in TD buffer (20 mM Tris-HCl, pH 8.0, containing 0.02 wt % β-DDM) (D–F). Fluorescence spectra upon excitation at 650 nm (B, C, E, and F) indicate quenching of ATTO fluorescence (B and E; blue and black traces correspond to T8C-ATTO and free ATTO at the same ATTO concentration as in T8C-ATTO, respectively) and concomitant enhancement of B850 fluorescence (C and F; blue and black traces correspond to T8C-ATTO and T8C at the same LH2 concentration as in T8C-ATTO, respectively).

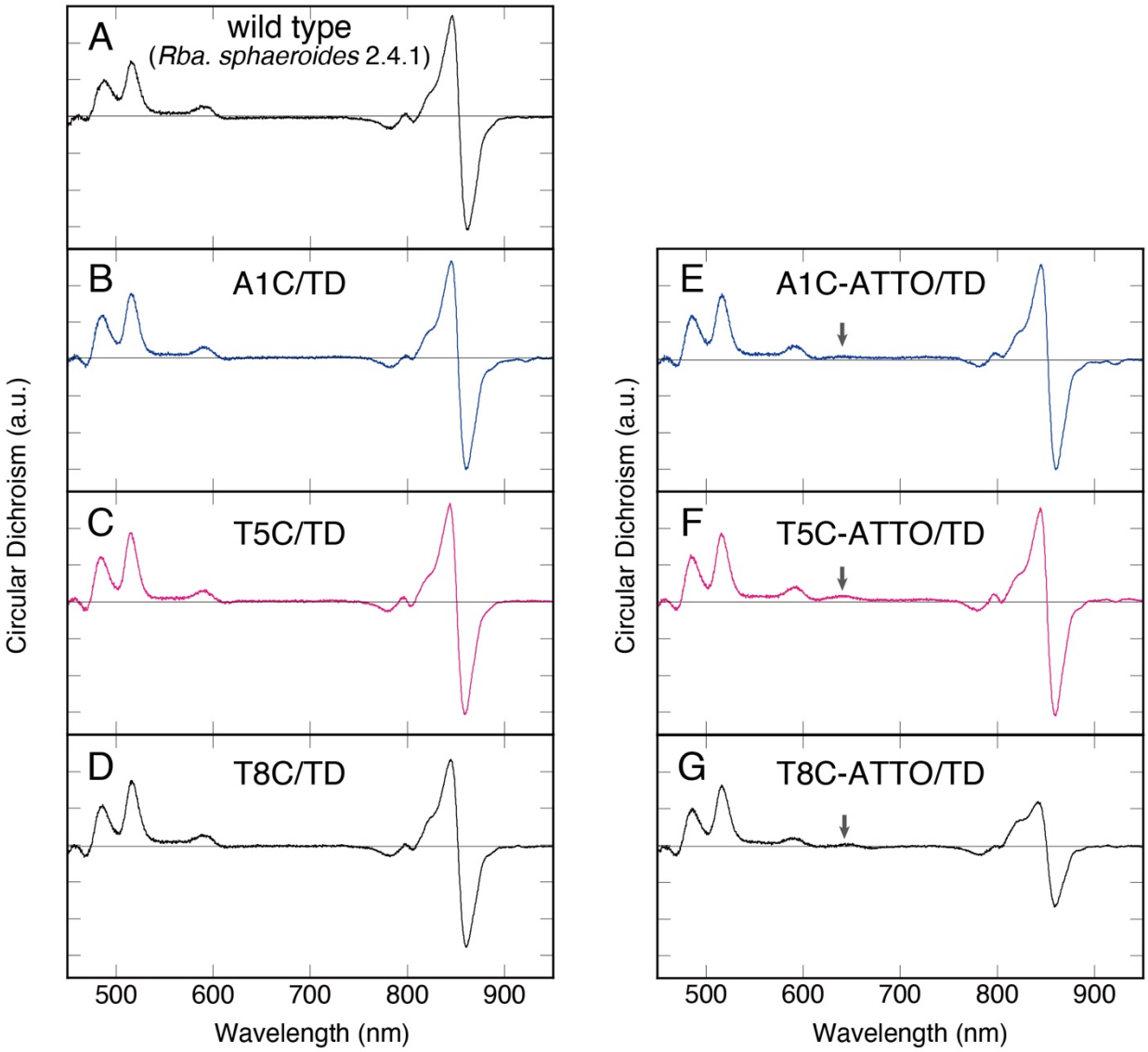

Figure S7. Circular dichroism spectra of LH2 complexes dissolved in TD buffer (20 mM Tris-HCl, pH 8.0, containing 0.02 wt % β-DDM): (A) wild-type LH2 (*Rba. sphaeroides* 2.4.1), (B) A1C, (C) T5C, (D) T8C, (E) A1C-ATTO, (F) T5C-ATTO, (G) T8C-ATTO. Arrows in panels E–G indicate a small ATTO-derived CD signal near 650 nm.

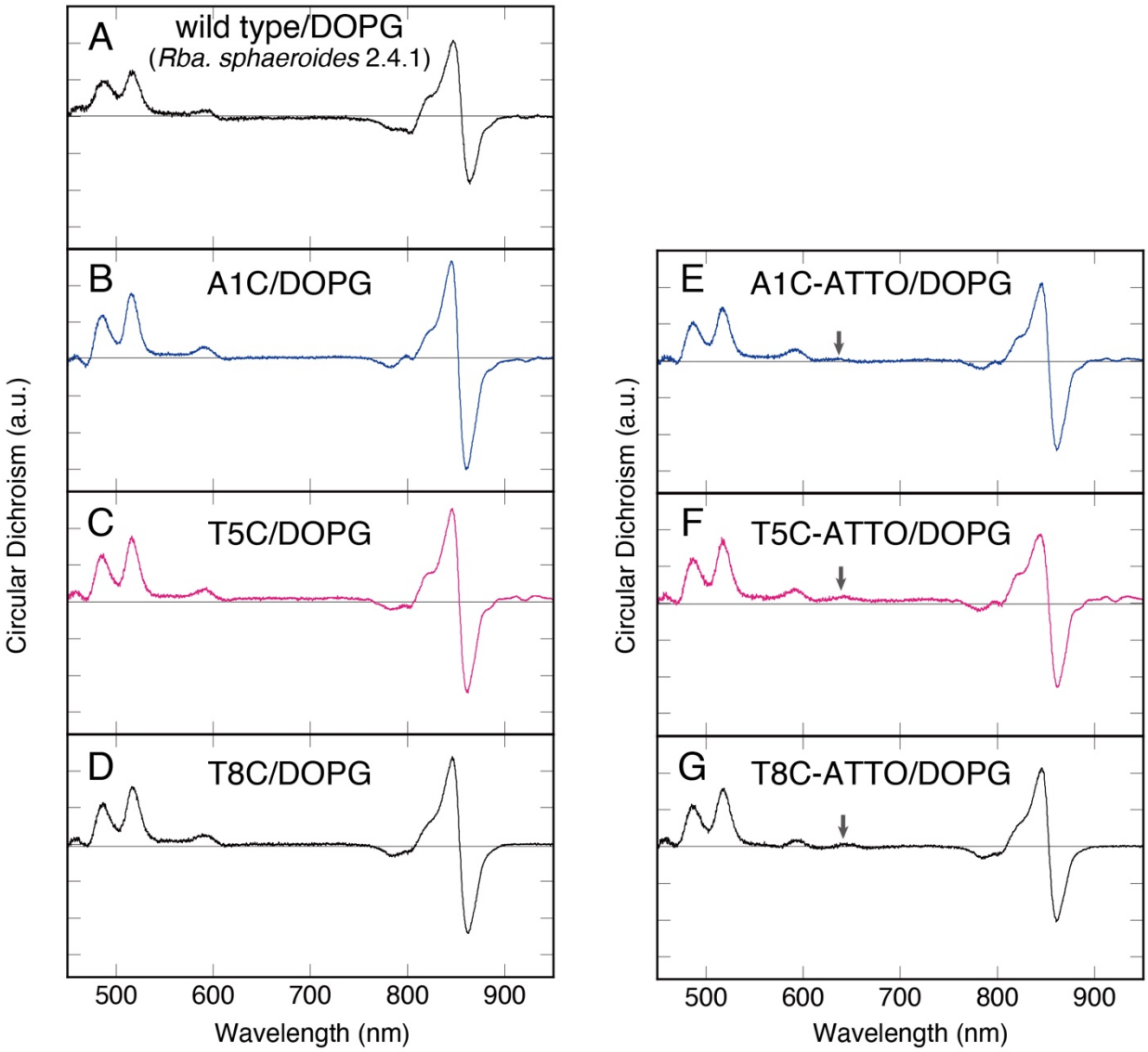

Figure S8. Circular dichroism spectra of LH2 complexes reconstituted into DOPG vesicles (20 mM Tris-HCl, pH 8.0): (A) wild-type LH2 (*Rba. sphaeroides* 2.4.1), (B) A1C, (C) T5C, (D) T8C, (E) A1C-ATTO, (F) T5C-ATTO, (G) T8C-ATTO. Arrows in panels E–G indicate a small ATTO-derived CD signal near 650 nm.

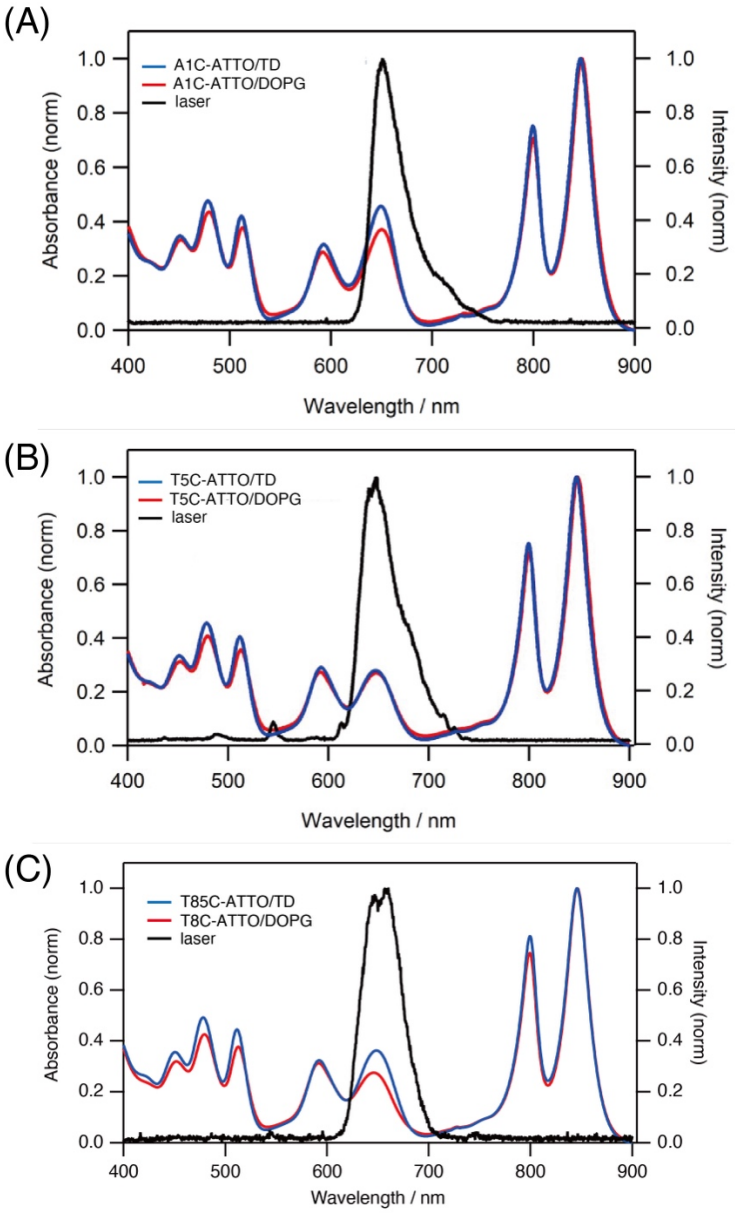

Figure S9. Absorption spectra of the LH2-ATTO conjugates overlaid with the excitation (pump) pulse spectra used for TA measurements: (A) A1C-ATTO, (B) T5C-ATTO, (C) T8C-ATTO. The pump pulse durations and average powers were 22 fs and 40 μW for (A), 20 fs and 40 μW for (B), and 19 fs and 5 μW for (C), respectively.

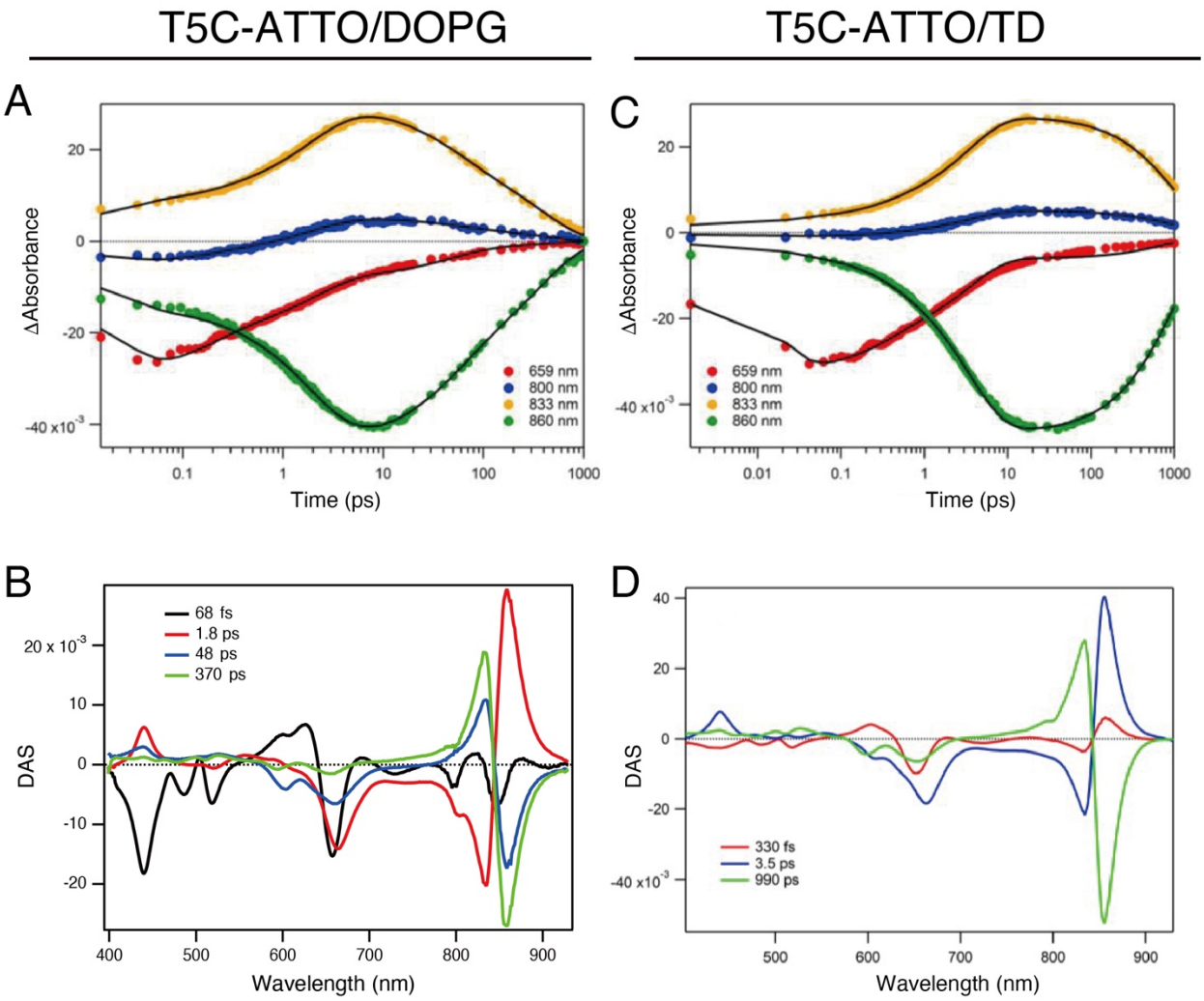

Figure S10. Time dependence of the ΔAbsorbance at four probe wavelengths with global fitting (A, C) and the corresponding decay-associated spectra (B, D) for T5C-ATTO/DOPG (A, B) and T5C-ATTO/TD (C, D). Excitation wavelength: 650 nm.

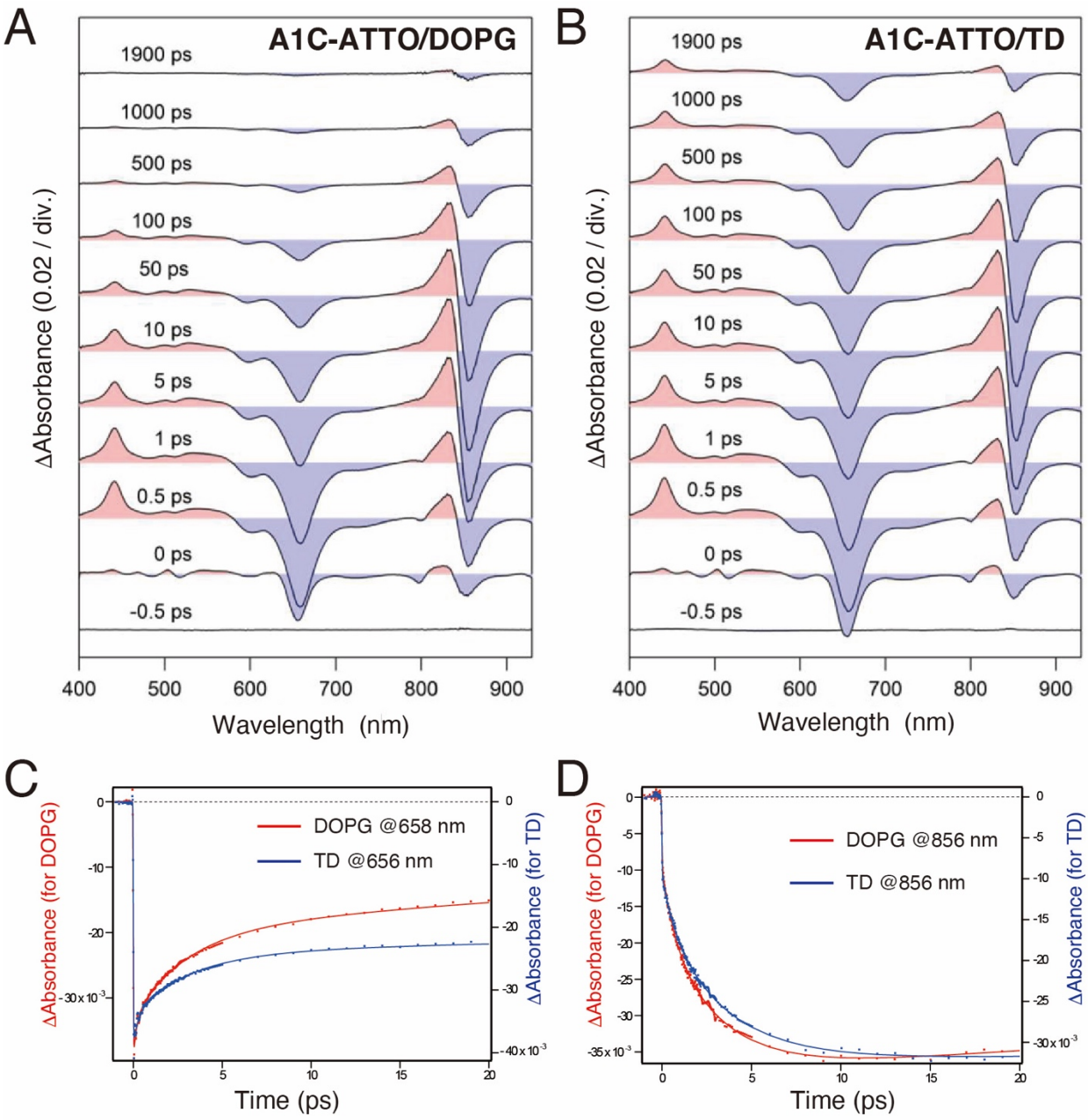

Figure S11. Transient absorption spectra of A1C-ATTO in DOPG-reconstituted (A, A1C-ATTO/DOPG) and detergent-solubilized (B, A1C-ATTO/TD) systems upon excitation at 650 nm. (C, D) Time dependence of ΔAbsorbance corresponding to ground state bleaching and stimulated emission of ATTO (C) and B850 (D) for the DOPG-reconstituted (red) and the detergent-solubilized (blue) systems. Fitted curves are shown as solid lines.

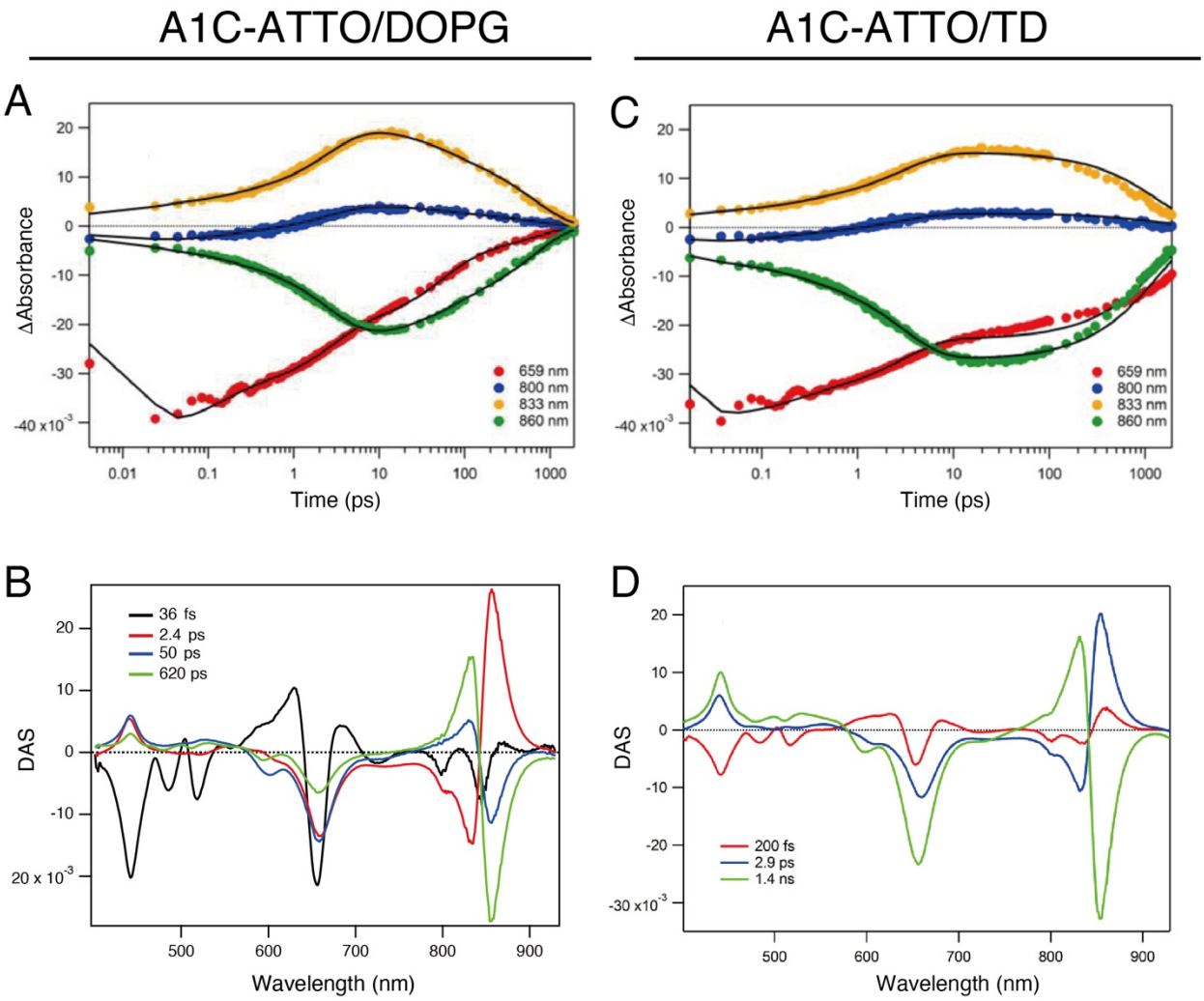

Figure S12. Time dependence of the ΔAbsorbance at four probe wavelengths with global fitting (A, C) and the corresponding decay-associated spectra (B, D) for A1C-ATTO/DOPG (A, B) and A1C-ATTO/TD (C, D). Excitation wavelength: 650 nm.

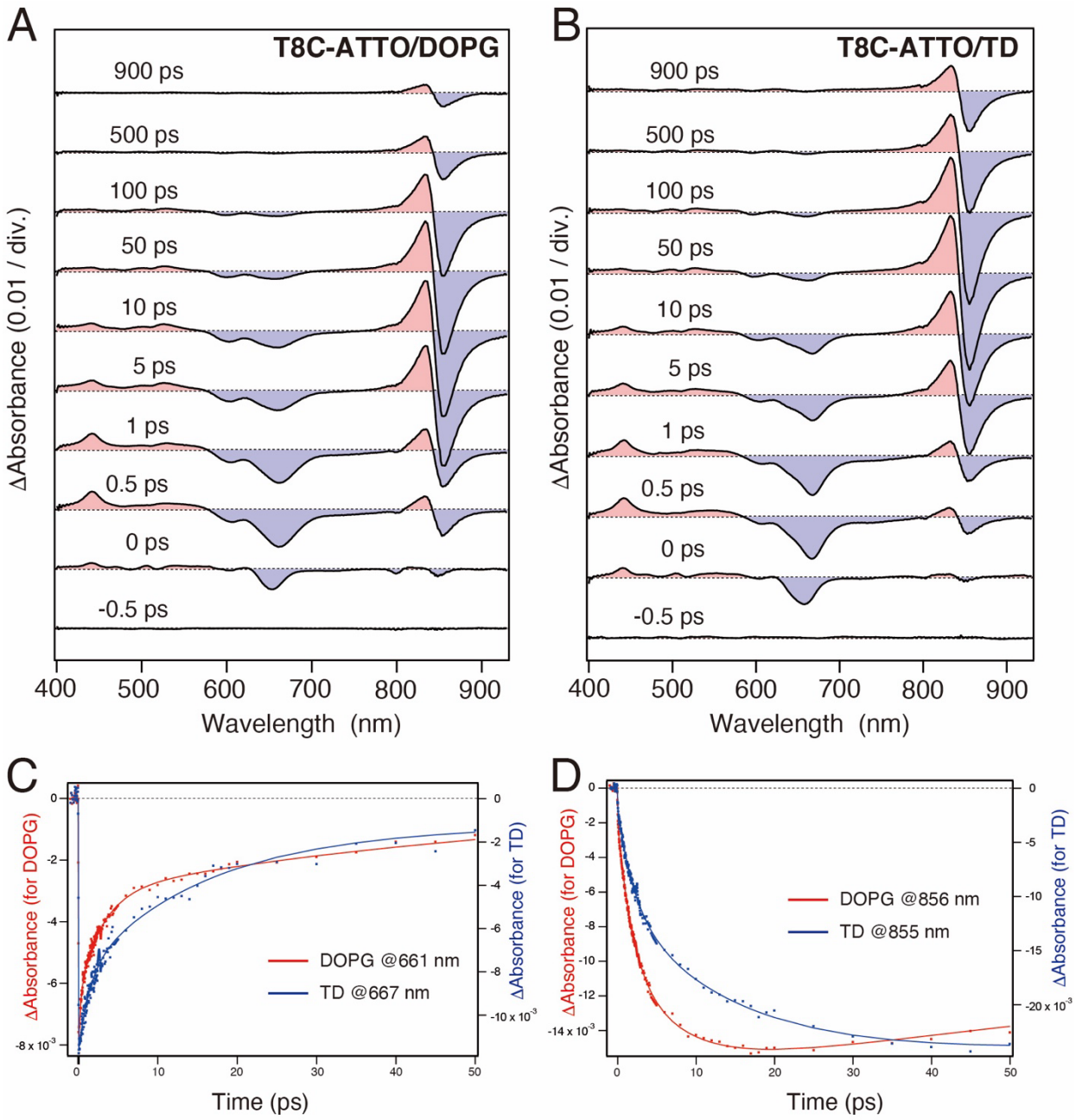

Figure S13. Transient absorption spectra of T8C-ATTO in DOPG-reconstituted (A, T8C-ATTO/DOPG) and detergent-solubilized (B, T8C-ATTO/TD) systems upon excitation at 650 nm. (C, D) Time dependence of ΔAbsorbance corresponding to ground state bleaching and stimulated emission of ATTO (C) and B850 (D) for the DOPG-reconstituted (red) and the detergent-solubilized (blue) systems.

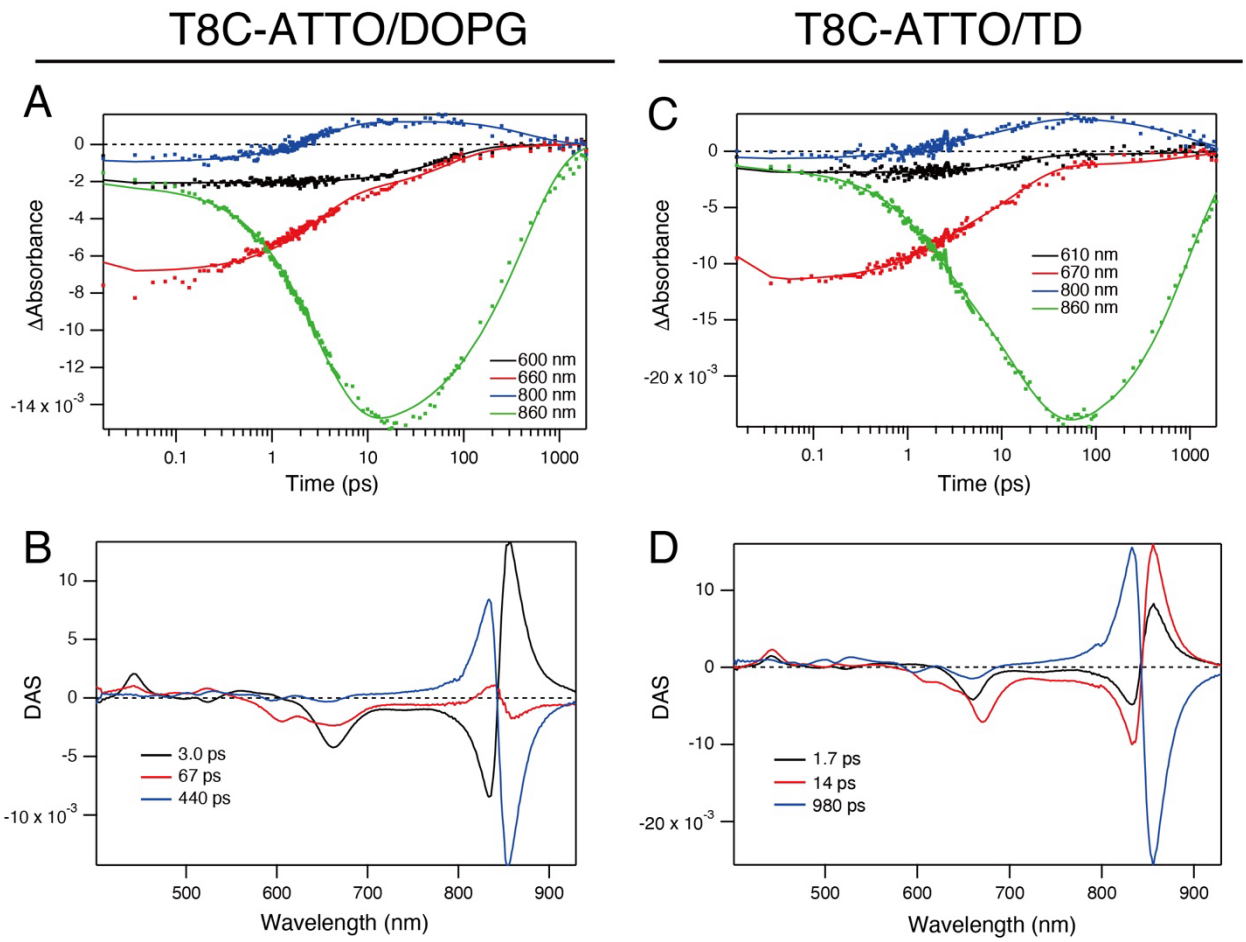

Figure S14. Time dependence of the ΔAbsorbance at four probe wavelengths with global fitting (A, C) and the corresponding decay-associated spectra (B, D) for T8C-ATTO/DOPG (A, B) and T8C-ATTO/TD (C, D). Excitation wavelength: 650 nm.

Table S2. Time constants obtained from Global Analysis for the biohybrid LH2s

System	Time constant (ps)		
DOPG-reconstituted	A1C	T5C	T8C
(Tris-HCl)	0.04	0.07	
	2.4	1.8	3
	50	48	67
	620	370	440
TD buffer	0.2	0.33	1.7
(Tris-HCl+β-DDM)	2.9	3.5	14
	1400	990	980

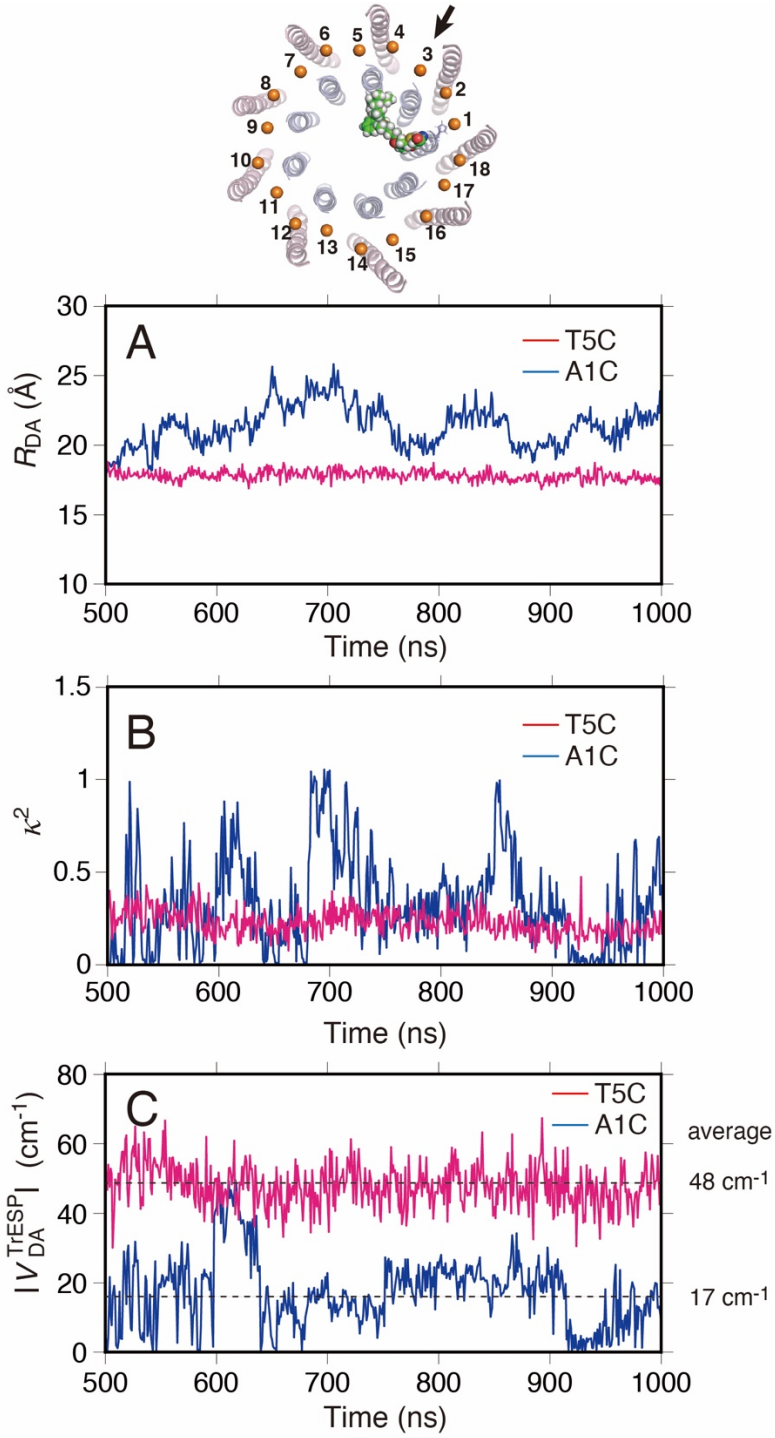

Figure S15. Donor–acceptor distance R_{DA} (A), orientation factor κ^2 (B), and electronic coupling $|V_{DA}^{TrESP}|$ (C) between ATTO and B850-BChl*a* **3** for T5C-ATTO and A1C-ATTO, plotted as a function of MD simulation time.

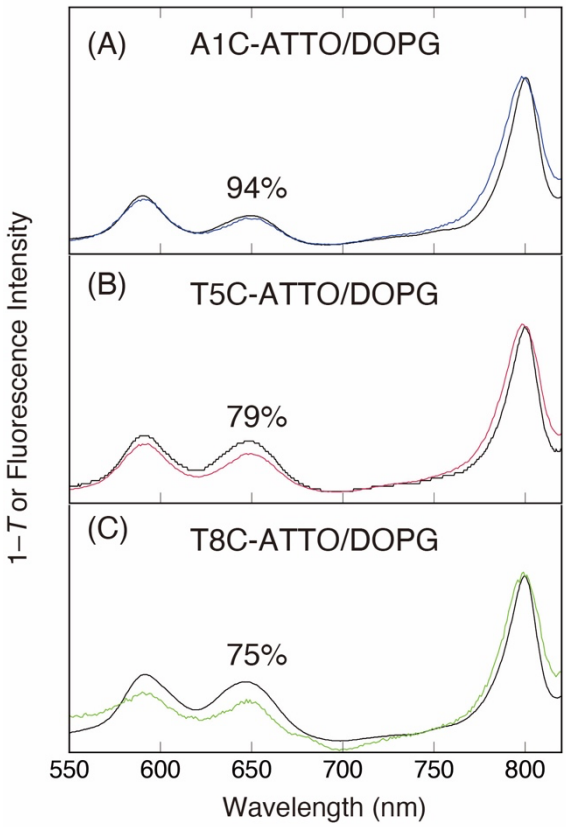

Figure S16. Fluorescence excitation spectra of A1C-ATTO/DOPG (A), T5C-ATTO/DOPG (B), and T8C-ATTO/DOPG (C) monitored at 880 nm. The excitation spectra (colored lines) were compared with absorptance (1 − T, T: transmittance) spectra (black lines), normalized at B800. The evaluated yields of energy transfer from ATTO to B850 are shown in the panels.